RSC Advances

PAPER

View Article Online
View Journal | View Issue

Cite this: *RSC Adv.*, 2018, **8**, 2138

Highly selective non-enzymatic electrochemical sensor based on a titanium dioxide nanowire–poly(3-aminophenyl boronic acid)–gold nanoparticle ternary nanocomposite

N. Muthuchamy,†[a] A. Gopalan†[ab] and Kwang-Pill Lee *[ab]

A novel three component (titanium dioxide nanowire (TiO_2 NW), poly(3-aminophenyl boronic acid) (PAPBA) and gold nanoparticles (Au NPs)) based ternary nanocomposite (TNC) (designated as TiO_2 NW/PAPBA–Au TNC) was prepared by a simple two-stage synthetic approach and utilized for the fabrication of a non-enzymatic (enzyme-free) glucose (NEG) sensor. In stage 2, the PAPBA–Au NC was formed by oxidative polymerization of 3-APBA using $HAuCl_4$ as oxidant on the surface of pre-synthesized TiO_2 NW *via* electrospinning (stage 1). The formation of PAPBA–Au NC as the shell on the surface of the TiO_2 NW (core) was confirmed by field emission scanning electron microscopy (FE-SEM). Notably, we obtained a good peak to peak separation, and a high peak current for the redox $Fe(CN)_6^{3-/4-}$ process indicating excellent electron transfer capability at the glassy carbon electrode (GCE)/TiO_2 NW/PAPBA–Au TNC interface. Also, the fabricated TiO_2 NW/PAPBA–Au TNC provides excellent electrocatalytic activity towards glucose detection in neutral (pH = 7.0) phosphate buffer solution. The detection of glucose was monitored using differential pulse voltammetry. The obtained sensitivity and detection limits are superior to many of the TiO_2 based enzymatic and non-enzymatic glucose sensors reported in the literature. Furthermore, the TiO_2 NW/PAPBA–Au TNC sensor is preferred because of its high selectivity to glucose in the presence of co-existing interfering substances and practical application for monitoring glucose in human blood serum samples.

Received 17th August 2017
Accepted 19th December 2017

DOI: 10.1039/c7ra09097h

rsc.li/rsc-advances

1. Introduction

Diabetes, a global health problem affecting over 200 million people, can cause disorders of the kidney, heart, neural system and retina.[1] Hence, the monitoring of blood glucose levels is essential to prevent diabetic complications such as diabetes from becoming more prevalent in modern society. Conventional glucose sensors use glucose oxidase immobilized on a solid electrode, to catalyze the oxidation of glucose in the presence of oxygen to produce hydrogen peroxide and selectively monitor the glucose levels.[2] Although such enzymatic glucose sensors are available commercially, they suffer from some limitations such as complex enzyme immobilization procedures, instability due to the intrinsic nature of enzymes, sensitivity to the chemical environment (*e.g.* pH), and temperature.[3] Besides, long-term monitoring of the blood glucose levels using an enzyme-based electrode is typically hampered by surface fouling by the absorption/passivation of the products. The surface fouling inevitably limits the selectivity and sensitivity towards glucose oxidation over time.[4,5] As a result, development of non-enzymatic glucose (NEG) sensors is becoming essential.[6]

Various nanostructured metals (*e.g.*, Au,[7] Pt,[8] Pd,[9] metal oxides (*e.g.*, NiO,[10] Co_3O_4,[11] CuO[12]), their composites (*e.g.*, CuO–SWCNT)),[13] and nanocomposites (Cu based multicomponent nanobead),[14] BiOCl–G nanohybrid sheets,[15] CuO–MWCNT[16] had been used to fabricate NEG sensors. A comprehensive review has been published on the fabrication of NEG sensors using various nanomaterials.[17] Among the metal oxide nanostructures based sensors, TiO_2 nanostructures have attracted much interest due to their combinational properties such as high surface area, electrocatalysis, non-toxicity, biocompatibility, and oxygen storage capacity. However, pristine TiO_2 electrodes usually have poor electrochemical activity because of the low conductivity of TiO_2.[18,19] Nanocomposites of TiO_2, such as TiO_2 modified with metal nanoparticles, are thus promising in NEG sensors.[20] Several binary composites based on TiO_2 such as TiO_2–G,[21] NiO–TiO_2,[22] TiO_2/CuO[23] and TiO_2/Pd,[24] TiO_2/Co_3O_4 (ref. 25 and 26) were used for the fabrication of NEG sensors. One dimensional (1D) nanostructures of TiO_2, specifically

[a]*Research Institute of Advanced Energy Technology, Kyungpook National University, Daegu, South Korea. E-mail: kplee@knu.ac.kr*

[b]*Department of Nanoscience and Nanotechnology, Kyungpook National University, Daegu, South Korea*

† Authors contributed equally to this work.

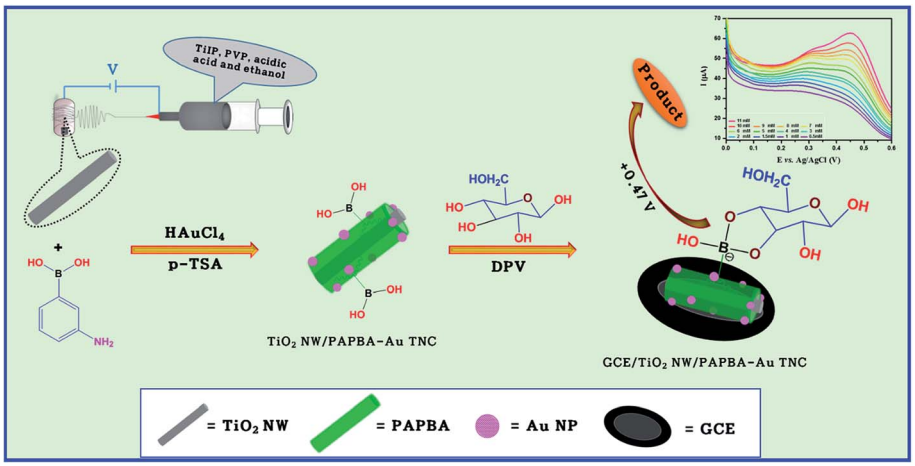

Scheme 1 Schematic diagram of the preparation of TiO_2 NW/PAPBA–Au TNC and electrochemical performance towards glucose detection.

nanowires (NW), possess essentially the common physical characteristics as that of 2D and 3D nanostructures of TiO_2, but geometrically offer the additional advantages like good transport of electrons and mechanical stability.[27] 1D TiO_2 NWs, could also be integrated with other materials or nanomaterials to improve the surface area and electron transport properties. Our recent research studies demonstrated that TiO_2 based nanocomposite can serve as the highly sensitive electrode for the determination of cholesterol and nitrate ions.[28,29] However, studies on the use of TiO_2 NW in combination with a glucose selective polymer towards NEG sensor has not been reported so far.

Boronic acid is well known to interact with 1,2- or 1,3-diols, at physiological pHs or above, and form reversible covalent bonds to generate five or six-membered cyclic complexes.[30] The chemical interactions between boronic acid and diols have been utilized for the detection of diol-containing biomolecules, such as sugars, dopamine, glycoproteins, and bacteria.[31–33] Boronic acid groups containing polymers such as poly(3-aminophenyl boronic acid) (PAPBA) have exhibited good operational stability and selectivity towards detection of glucose levels as compared to glucose oxidase and hence utilized for the fabrication of NEG sensors.[34–37] Due to their fascinating electrical and catalytic properties, gold nanoparticles (Au NPs) have been utilized widely in electrochemical applications.[38–40] Au NPs in combination with G (carbon 98, 90 (2016)); calix[41] arene/boronic acids[42] were used to improve the performance of NEG sensors.

In this background, we have constructed the NEG sensor based on a new ternary nanocomposite (TNC) comprised of TiO_2 NW, Au NPs and PAPBA (designated as TiO_2 NW/PAPBA–Au TNC) (Scheme 1). Firstly, 1D TiO_2 NWs were synthesized by electrospinning and hydrothermal processes.[43] Followed by the synthesis of TiO_2 NWs, Au NPs distributed PAPBA NC was formed on the surface of TiO_2 NW by a one-step polymerization of 3-APBA using auric chloride ($HAuCl_4$) as the oxidizing agent. The morphology and electrochemical properties of TiO_2 NW/PAPBA–Au TNC were investigated by field emission scanning electron microscopy (FE-SEM) electrochemical impedance spectroscopy (EIS) and cyclic voltammetry (CV). The fabricated NEG sensor based on GCE/TiO_2 NW/PAPBA–Au TNC electrode exhibited excellent performances towards electrochemical glucose detection (Scheme 1), including high sensitivity and good selectivity in the presence of common interfering species as compared to the pristine components, PAPBA and TiO_2 NW, as well over the glucose sensing performances based on other TiO_2 based materials reported in literature (Table 1). Moreover, the capability of utilizing GCE/TiO_2 NW/PAPBA–Au TNC electrode for determination of glucose levels in human serum is demonstrated, suggesting the potential of the fabricated NEG sensor for practical diabetes diagnosis.

Table 1 Comparison of glucose sensor analytical performances between GCE/TiO_2 NW/PAPBA–Au TNC, PAPBA–Au NC electrodes fabricated in this work and other glucose sensors

Glucose sensor	Sensitivity [$\mu A\ cm^{-2}\ mM^{-1}$]	Linear range [mM]	Reference
GOx/PANI-NF/GCE	—	0.01–1.0	44
Cyt c/AuNPs/PANI-NS	63.1	0.01–3.2	45
PANI-NT/GOx	4.62	0.01–5.5	46
GOx/n-TiO_2/PANI/GCE	6.31	0.02–6.0	47
Pt/CNTs/TiO_2 NTAs	0.24	0.006–1.5	48
GOx/TiO_2/CNTs	11.3 ± 1.3	Up to 3.0	49
TiO_2–SWCNT NWS	5.32	0.010–1.42	50
Cu_2O/TiO_2	14.56	3.0–9.0	51
GOx/Ag/TiO_2 NTAs	0.39	0.1–4.0	52
GOx/Pt/Gr/TiO_2 NTAs	0.94	0.1–8.0	53
AuNPs–TiO_2 NT	—	0.40–8.0	54
TiO_2–GR	6.20	0–8.0	21
Chitosan–AuNPs	—	0.006–0.14	55
GOD/1DH S–TiO_2	9.9	0.2–1.0	56
GOD/HNF–TiO_2/GC	32.6	0.002–3.17	57
Nafion-silica/ MWCNTs-*g*-PANI/GOx	5.01	1–10	58
GCE/PAPBA–Au NC	34.6	0.5–11.0	This work
GCE/TiO_2 NW/ PAPBA–Au TNC	66.8	0.5–11.0	This work

2. Experimental details

2.1. Chemicals

$HAuCl_4$, *p*-toluenesulfonic acid (*p*-TSA), 3-APBA, Ti(IV) isopropoxide, polyvinylpyrrolidone (PVP, molecular weight < 40 000, Fluka) acetic acid, glucose and human serum (from human male AB plasma, USA origin, sterile-filtered) were purchased from Sigma-Aldrich, South Korea and used as received. Ammonium peroxydisulfate (APS) was obtained from Samchum Chemicals, South Korea. Phosphate buffer solution (PBS, pH = 7) and ethanol were obtained from OCI Company Ltd., South Korea.

2.2. Formation of TiO_2 NW/PAPBA–Au TNC

The formation stages of TiO_2 NW/PAPBA–Au TNC include: (i) preparation of TiO_2-NWs and (ii) simultaneous formation of PAPBA and Au NPs on TiO_2 NW.

2.2.1. Preparation of TiO_2 NW. The details of the preparation of pristine TiO_2 NW are similar to that reported in our previous publication.[43] In a typical procedure for the preparation of TiO_2 NW, firstly, the composite titanate nanofibers were obtained by electrospinning a sol–gel-transformed electrospinning dope. The electrospinning dope was prepared using PVP, TiIP, acetic acid, and ethanol as follows. TiIP (2 mL) and PVP (4 g) were added to an acetic acid : ethanol (3 : 7 v/v) 18 mL solution and stirred for 2 h. The resulting electrospinning dope was transferred into a plastic syringe equipped with a needle (0.25 mm diameter) and subjected to electrospinning by applying a DC voltage of 25 kV using a programmable syringe pump at a flow rate of 0.7 mL h^{-1}. The composite titanate nanofibers were collected on a grounded rotating drum covered with an aluminum foil placed at a distance of 15 cm from the spinneret. The composite titanate nanofibers were sintered by calcination in air at 500 °C for 3 h. The calcined materials, TiO_2-NWs, was collected and washed with ethanol to remove impurities.

2.2.2. Formation of PAPBA–Au NC on TiO_2 NW. A solution containing 3-APBA (50 mM) and 10 mg of TiO_2-NWs was prepared in 0.1 M *p*-TSA and stirred for 1 h. About 10 mL of aqueous $HAuCl_4$ (5 mM) was added dropwise to the above solution. The reaction was allowed to proceed for 24 h under stirring. The dark green precipitate, (TiO_2 NW/PAPBA–Au TNC) was washed several times with distilled water and dried at 60 °C in an air oven. For the comparison purposes, PAPBA–Au NC was prepared by performing the polymerization of APBA using $HAuCl_4$ in the absence of TiO_2 NW. Pristine PAPBA was prepared as follows; a solution of 3-APBA (40 mL) was prepared in 0.1 M *p*-TSA. And, about 10 mL of 0.25 M of APS solution was added dropwise into 3-APBA solution maintained at ~5 °C and the mixture was stirred for 24 h. The precipitate (PAPBA) was washed with water and dried at 60 °C in an air oven. TiO_2 NW/PAPBA–Au TNC was prepared by carrying out the polymerization of 3-APBA in the presence of TiO_2 NW using APS as the oxidant.

2.3. Fabrication of modified electrodes for NEG sensing

TiO_2 NW/PAPBA–Au TNC, PAPBA–Au NC, TiO_2 NW/PAPBA NC and pristine PAPBA modified electrodes were prepared by dispersing 2 mg of the respective electrode modifying the material in 0.1 mL of isopropyl alcohol and Nafion (3 : 2 v/v) solution. The mixture was sonicated for 10 min to obtain an ink. About, 6 μL of the ink was dropped on the surface of polished glassy carbon electrode (GCE, area = 0.07065 cm^2) and dried at room temperature.

2.4. Morphological characterization

Field emission scanning electron microscopy (FE-SEM) coupled with energy dispersive X-ray (EDX) (Hitachi S-4300, Japan) analysis was used to study morphology and elemental composition. The crystal structure of the prepared materials was investigated by X-ray diffraction (XRD, Quantera SXM, ULVAC-PHI, Japan) using Cu Kα radiation (λ = 1.5406 Å) in the 2θ range of 20–85°.

2.5. Electrochemical properties and NEG sensing

Electrochemical measurements were performed using Ivium-Stat (Netherland) electrochemical interface with PC-controlled analyzer workstation. A conventional three-electrode cell assembly was used. The modified electrode was used as the working electrode. Ag/AgCl and platinum wire were used as reference and counter electrodes, respectively. The electroactivity of the modified electrodes was evaluated using cyclic voltammetry in 0.1 M PBS (pH 7). The glucose detection experiments were carried out using differential pulse voltammetry measurements at a scan rate of 0.05 V s^{-1} with a pulse amplitude of 0.05 V, pulse rate of 0.5 s and pulse width of 50 ms for various glucose concentrations in an electrochemical cell containing a magnetically stirred PBS electrolyte.

3. Result and discussion

3.1. Morphology and structural characterization

The morphologies of the as-prepared TiO_2 NW/PAPBA–Au TNC, PAPBA–Au NC, TiO_2 NW/PAPBA NC and pristine PAPBA were characterized by FE-SEM analysis. As shown in the FE-SEM image of TiO_2 NW/PAPBA–Au TNC (Fig. 1a), the smooth surface of TiO_2 NW (Fig. 1a, inset) was transformed into an uneven and bumpy surface, suggested that the surface of TiO_2 NW was completely covered with PAPBA–Au NC. On close perusal of the surface of TiO_2 NW/PAPBA–Au TNC (Fig. 1a), one can identify two kinds of materials, spherical bright dots (Au NPs) and the dark puffy mass (PAPBA). It is clear that Au NPs were distributed within PAPBA matrix and existed on the surface of TiO_2 NW. EDAX analysis of the TiO_2 NW/PAPBA–Au TNC informed that nearly 17.63 wt% of elemental Au is presented in (Fig. 2). Thus, the treatment of $HAuCl_4$ with 3-APBA in the presence of TiO_2 NW modified the TiO_2 NW surface with a PAPBA–Au shell layer. FESEM image of TiO_2 NW/PAPBA NC (Fig. 1b) also reveals the modification of the surface of TiO_2 NW. In this case, a much increased (about 150 nm thick) shell layer of PAPBA was formed on TiO_2 NW surface. Fig. 1c displays the image of PAPBA–Au NC with the distribution of larger sized spherical Au NPs (diameters in the range 130–200 nm) on the

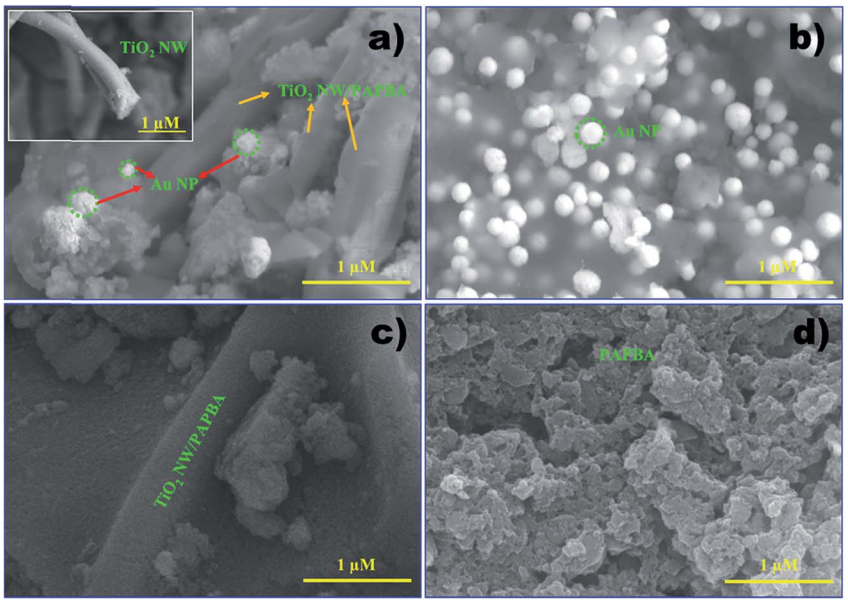

Fig. 1 FE-SEM images of (a) TiO_2 NW/PAPBA–Au TNC, (inset: image of TiO_2 NW) (b) PAPBA–Au NC, (c) TiO_2 NW/PAPBA NC, (d) pristine PAPBA.

amorphous host matrix of PAPBA with minimum aggregations. The pristine PAPBA had a granular morphology (Fig. 1d).

Fig. 3 shows the XRD patterns of the TiO_2 NW/PAPBA–Au TNC (Fig. 3a), PAPBA–Au NC (Fig. 3b). The XRD pattern of TiO_2 NW/PAPBA–Au TNC (Fig. 3a) exhibits peaks centered at 2θ = 27.48°, 36.18°, 38.24°, 54.46°, 56.68°, 62.96°, 69.08° and 69.86° that correspond to (110), (103), (004), (211), (220), (204), (116) and (112) reflections of anatase TiO_2, peaks corresponding to the atomic planes of Au [2θ = 44.56° (200), 64.82° (220), and

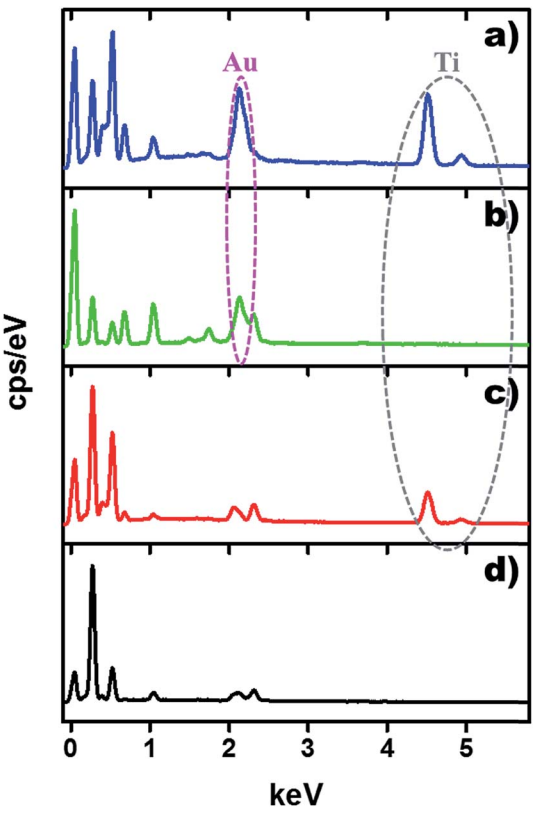

Fig. 2 EDX spectrum of the TiO_2 NW/PAPBA–Au TNC, PAPBA–Au NC, TiO_2 NW/PAPBA NC, pristine PAPBA.

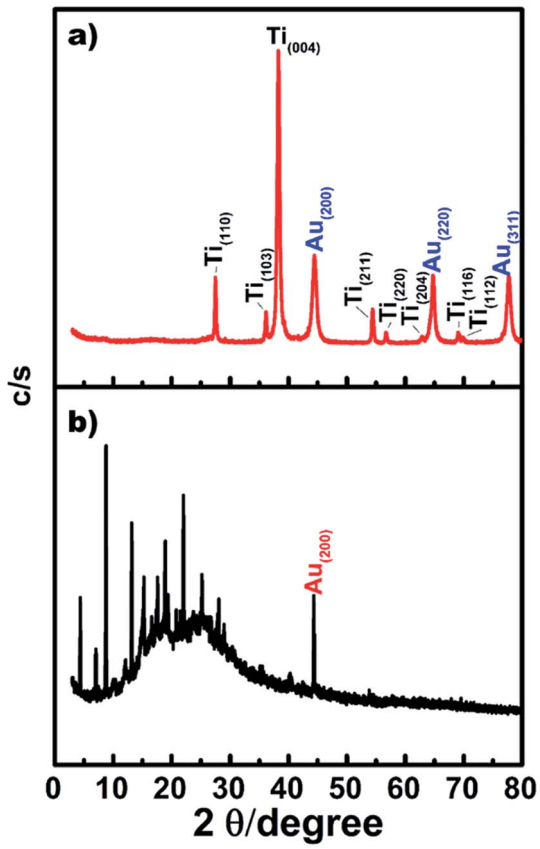

Fig. 3 XRD pattern of the TiO_2 NW/PAPBA–Au TNC, PAPBA–Au NC.

77.68° (311)] and a broad band around 10–25°. The XRD pattern of PAPBA–Au NC (Fig. 3b) comprises of an intense broadband around $2\theta = 10–25°$ (PAPBA) that is attributed to the periodically parallel chain of amorphous polymers of PAPBA and a sharp peak Bragg reflection peak at $2\theta = 44.56°$ (Au (200)). The Au reflection peaks at 38.24° (100) and 64.8° (220) are less intense as compared to XRD pattern of the TiO_2 NW/PAPBA–Au TNC (Fig. 3a). Thus, XRD pattern of TiO_2 NW/PAPBA–Au TNC (Fig. 3a) corroborates with the coexistence of crystalline TiO_2, Au atomic planes, and amorphous PAPBA.

3.2. Electrochemical properties

3.2.1. Electroactivity. The electroactivity, in terms of efficiency of the electron transport across the electrode/modifying material interface, was monitored for the fabricated modified electrodes using the bench mark redox couple $Fe(CN)_6^{3-/4-}$, by recording cyclic voltammograms (CVs) in the potential range from −0.20 V to 0.60 V, over the scan rates ranging from 0.02 V s^{-1} to 0.2 V s^{-1} at the GCE/TiO_2 NW/PAPBA–Au TNC (Fig. 4a), GCE/PAPBA–Au NC (Fig. 4b), GCE/TiO_2 NW/PAPBA NC (Fig. 4c) and GCE/pristine PAPBA (Fig. 4d) electrodes. The CV of the bare GCE (Fig. 4a (inset)) in the presence of 5 mM of $Fe(CN)_6^{3-/4-}$ (0.1 M KCl) is also presented for a comparative purpose. Typically, the modified electrodes exhibited the $Fe(CN)_6^{3-/4-}$ redox transition peaks (Fig. 4a–d) as similar to the redox transitions noticed at the bare GCE (Fig. 4a (inset)). However, there are distinct differences between the anode peak to cathode peak separation (ΔE_p) and the anodic peak current (I_{pa})/cathodic peak currents (I_{pc}). The ΔE_p of the GCE/TiO_2 NW/PAPBA–Au TNC, GCE/PAPBA–Au NC, GCE/TiO_2 NW/PAPBA NC and GCE/pristine PAPBA electrodes were determined to be 0.04 V, 0.09 V, 0.27 V and 0.26, respectively, at a scan rate 20 mV s^{-1}. And, the GCE/TiO_2 NW/PAPBA–Au TNC electrode (I_{pa} = 3.124 μA) exhibited nearly 1.8, 1.44 and 1.66 times higher I_{pa} as compared to GCE/PAPBA–Au NC, GCE/TiO_2 NW/PAPBA NC, and GCE/pristine PAPBA electrode, respectively. The I_{pa}/I_{pc} linearly increased with the scan rate in the range of 0.02 to 0.2 V s^{-1} (Fig. 4, insets) and accompanied with a positive shift in the anodic peak and the negative shift in the cathodic peak of the $Fe(CN)_6^{3-/4-}$ redox process at modified electrodes. Furthermore, with the increase in scan rate (0.02–0.2 V s^{-1}), the ΔE_p increased steadily with nearly a constant I_{pa}/I_{pc} ratio. These results suggested the quasi-reversible one-electron behavior for the $Fe(CN)_6^{3-/4-}$ redox process at the modified electrodes. The electrochemically accessible surface area is an important empirical parameter to understand the relationship between the specific electrode activity and the structure/composition of the catalytic materials. The effective electroactive surface area (A) of the modified electrodes was calculated by using the Randles–Sevcik equation.[29] The A value for the GCE/TiO_2 NW/PAPBA–Au TNC, GCE/PAPBA–Au NC, GCE/TiO_2 NW/PAPBA NC, GCE/pristine PAPBA was calculated to be 8.22 cm^2, 5.40 cm^2, 5.06 cm^2 and 4.67 cm^2, respectively. The A value of GCE/TiO_2 NW/PAPBA–Au TNC is 1.55, 1.62 and 1.76 times higher than that of GCE/PAPBA–Au NC, GCE/TiO_2 NW/PAPBA NC, GCE/pristine PAPBA. Based on the results on

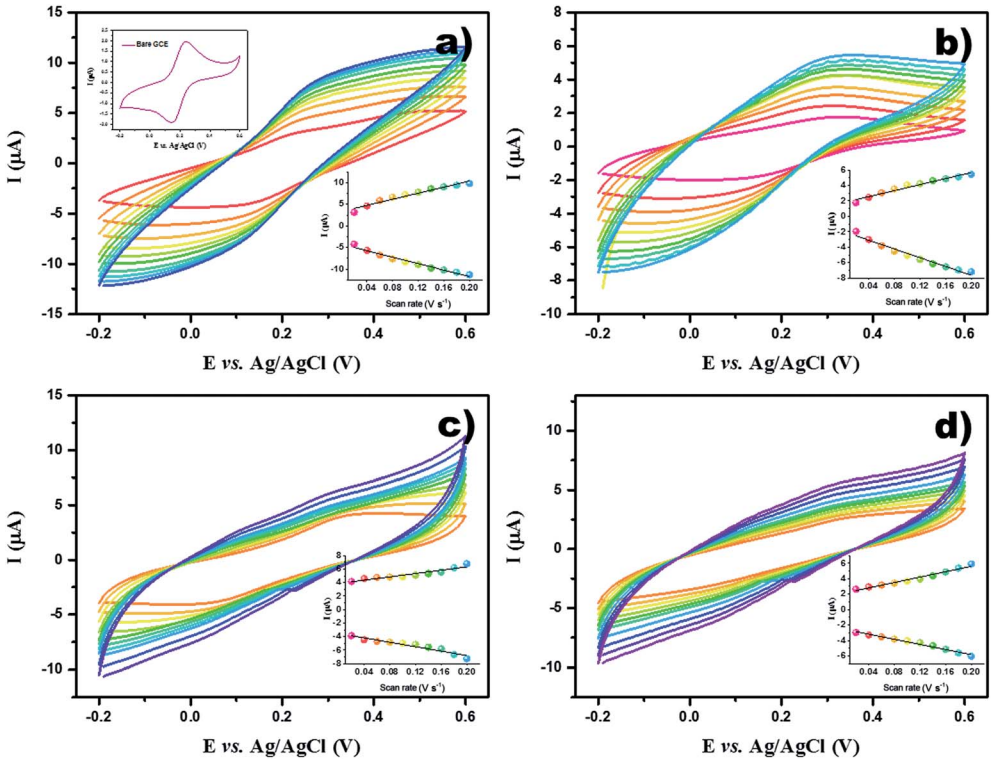

Fig. 4 CV curves for 5 mM of $Fe(CN)_6^{3-/4-}$ (0.1 M KCl) at different scan rate from 0.02 V s^{-1} to 0.20 V s^{-1} at the modified electrodes GCE/TiO_2 NW/PAPBA–Au TNC (a), GCE/PAPBA–Au NC (b), GCE/TiO_2 NW/PAPBA NC (c), GCE/pristine PAPBA (d) and bare GCE (a, inset).

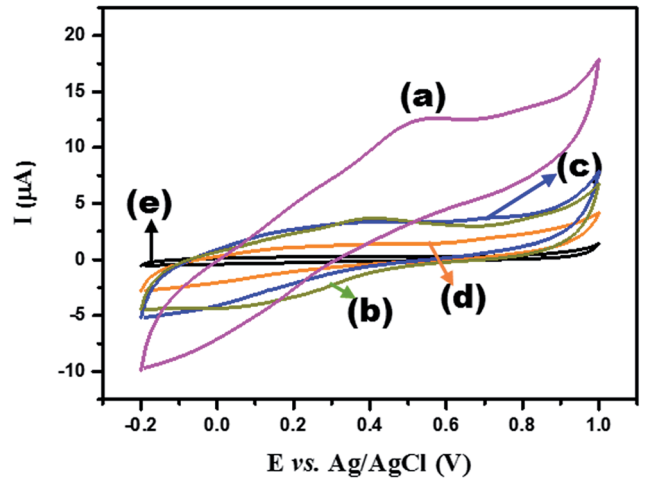

Fig. 5 CV curves of GCE/TiO_2 NW/PAPBA–Au TNC (a), GCE/PAPBA–Au NC (b), GCE/TiO_2 NW/PAPBA NC (c), GCE/pristine PAPBA (d) and bare GCE (e) electrodes recorded in 0.1 M PBS (pH 7) solution. Scan rate: 50 mV s^{-1}.

electroactivity of modified electrodes, it can be concluded that GCE/TiO_2 NW/PAPBA–Au TNC electrode has the larger surface area, lower ΔE_p and higher I_{pa}/I_{pc}, suggesting a faster electron transfer kinetics at the GCE/TiO_2 NW/PAPBA–Au TNC electrode. And, the electrode properties of GCE/TiO_2 NW/PAPBA–Au TNC (Fig. 5a), GCE/PAPBA–Au NC (Fig. 5b), GCE/TiO_2 NW/PAPBA (Fig. 5c), GCE/pristine PAPBA (Fig. 5d) and bare GCE (Fig. 5e) were evaluated in 0.1 M PBS (pH = 7) solution. Typically, the anodic peak current at the modified electrodes was compared with the bare GCE electrode. The anodic peak current (at +0.50 V, the scan rate of +0.05 V s^{-1}) showed the trend: GCE/pristine PAPBA < GCE/TiO_2 NW/PAPBA NC < GCE/PAPBA–Au NC < GCE/TiO_2 NW/PAPBA–Au TNC. To specifically note, the anodic current at GCE/TiO_2 NW/PAPBA–Au TNC is the largest among the modified electrodes.

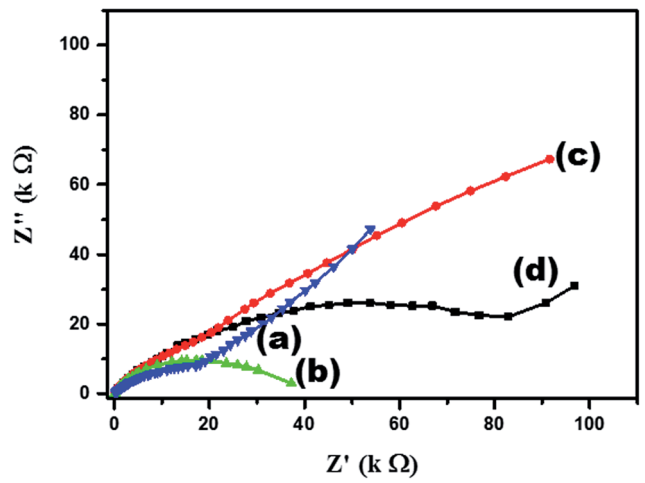

Fig. 6 Nyquist plots (*Z′ versus Z″*) of GCE/TiO_2 NW/PAPBA–Au TNC (a), GCE/PAPBA–Au NC (b), GCE/TiO_2 NW/PAPBA NC (c) and GCE/pristine PAPBA (d) electrodes recorded in 5 mM of $Fe(CN)_6^{3-/4-}$ (0.1 M KCl).

3.2.2. Interfacial properties. Electrochemical impedance spectroscopy (EIS) is an important electrochemical tool, which can be useful to understand the charge transfer resistance at the electrode and electrolyte interface of the modified electrodes. The diameter of the semicircle in a Nyquist plot is a direct measure of charge transfer resistance (R_{ct}). Fig. 6 presents of Nyquist plots of GCE/TiO_2 NW/PAPBA–Au TNC (Fig. 6a), GCE/PAPBA–Au NC (Fig. 6b), GCE/TiO_2 NW/PAPBA NC (Fig. 6c) and GCE/pristine PAPBA (Fig. 6d) electrodes recorded in 5 mM of $Fe(CN)_6^{3-/4-}$ (0.1 M KCl). Fig. 5 clearly informs that the GCE/TiO_2 NW/PAPBA–Au TNC electrode has the lowest R_{ct} (31.8 kΩ) among the other electrodes; GCE/PAPBA–Au NC (41 kΩ, Fig. 6b), GCE/TiO_2 NW/PAPBA NC (46 kΩ, Fig. 6c) and GCE/pristine PAPBA (97 kΩ, Fig. 6d), suggesting that the TiO_2 NW/PAPBA–Au TNC film significantly improves the conductivity and electron transfer process. Therefore, the GCE/TiO_2 NW/PAPBA–Au TNC electrode was selected as the most suited modified electrode for electrochemical detection of glucose.

3.3. NEG sensor performances

3.3.1. Electrocatalytic oxidation of glucose. As compared to cyclic voltammetry, the other electrochemical technique, differential pulse voltammetry, is less likely to get affected by the capacitive current. Differential pulse voltammetry measures only the difference between the current at the beginning and end of each pulse. We employed differential pulse voltammetry to monitor the faradaic current response of modified electrodes in the presence and absence of glucose (Fig. 7) at the optimized differential pulse voltammetric conditions. Fig. 7 depicts the differential pulse voltammograms (DPVs) obtained at the GCE modified with TiO_2 NW/PAPBA–Au TNC, PAPBA–Au NC, TiO_2 NW/PAPBA NC, and pristine PAPBA in the presence of 1 mM glucose (Fig. 7a′–d′ curves) and absence of glucose (Fig. 7a–e

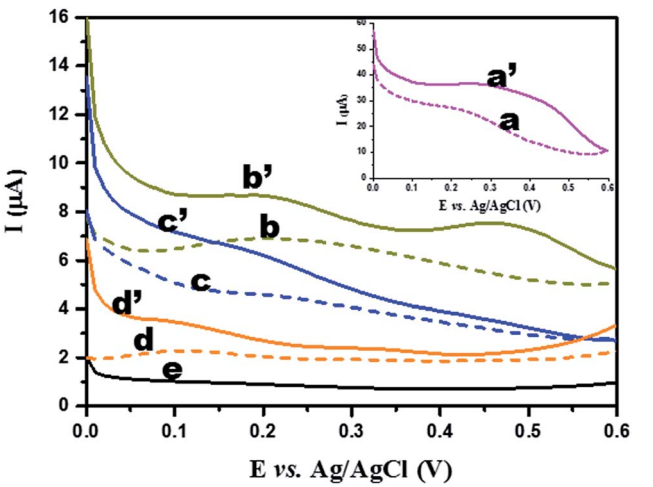

Fig. 7 DPV of glucose oxidation of GCE/TiO_2 NW/PAPBA–Au TNC (a and a′), GCE/PAPBA–Au NC (b and b′), GCE/TiO_2 NW/PAPBA NC (c and c′), GCE/pristine PAPBA (d and d′) and bare GCE (e) in 1 mM glucose + 0.1 M PBS solution (solid lines; a′–d′) and absence of glucose (dashed lines; a–e). Scan rate: 0.05 V s^{-1}, pulse amplitude: 0.05 V, pulse width: 50 ms.

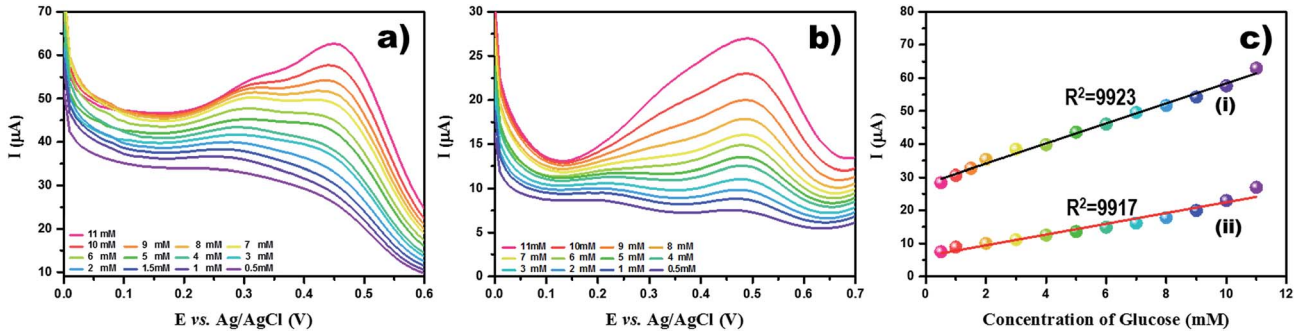

Fig. 8 DPV for various glucose concentration (0.5 to 11 mM) at (a) GCE/TiO_2 NW/PAPBA–Au TNC and (b) GCE/PAPBA–Au NC modified electrodes in phosphate buffer (pH 7). Scan rate: 50 mV s^{-1}, pulse amplitude: 50 mV, pulse width: 50 ms. (c) The plot of peak current *I* (mA) *versus* concentration glucose at (i) GCE/TiO_2 NW/PAPBA–Au TNC and (ii) GCE/PAPBA–Au NC modified electrodes.

curves) in 0.1 M PBS PBS solution (pH 7.0) at scan rate 0.05 V s^{-1}. The modified electrodes GCE/TiO_2 NW/PAPBA–Au TNC, GCE/PAPBA–Au NC, GCE/TiO_2 NW/PAPBA NC, and GCE/pristine PAPBA show much higher peak currents (beyond the potential of +0.25 V) as compared to the current responses in the absence of glucose. Especially, the as-prepared GCE/TiO_2 NW/PAPBA–Au TNC (Fig. 7a′) modified electrode exhibited an extraordinarily higher current response towards glucose oxidation than noticed at GCE/PAPBA–Au NC (Fig. 7b′), GCE/TiO_2 NW/PAPBA NC (Fig. 7c′) and GCE/pristine PAPBA (Fig. 7d′) modified electrodes. Typically, two distinct oxidation peaks were observed at around 0.20 V and 0.47 V for the GCE/TiO_2 NW/PAPBA–Au TNC electrode that corresponds to the oxidation of glucose to gluconolactone and oxidation of gluconolactone to the product, respectively. The DPV of the bare GCE (Fig. 7e) in the presence of glucose was featureless and informed that the bare GCE was completely electro inactive towards glucose oxidation in the potential range of interest. DPVs of the different concentrations of glucose, prepared by the proper dilution of stock glucose solution, were evaluated at GCE/TiO_2 NW/PAPBA–Au TNC (Fig. 8a) and GCE/PAPBA–Au NC (Fig. 8b). The size of the wave around 0.30 V to 0.50 V progressively increased and became sharper as the concentration of glucose increased for both modified electrodes (Fig. 8a and b). The height of peak current at +0.47 V was taken as the measure of quantifying the concentration of glucose. The exact current values at the GCE/TiO_2 NW/PAPBA–Au TNC (+0.47 V) were generated from the potentiostat. A good correlation was found between the concentrations of glucose and peak currents (Fig. 8c). Typically, the glucose oxidation peak current showed a linear increase with glucose concentration for the range between 0.5 and 11 mM at GCE/TiO_2 NW/PAPBA–Au TNC (Fig. 8c(i)) and GCE/PAPBA–Au NC (Fig. 8c(ii)) with correlation coefficients (R^2) as 0.9923 and 0.9917, respectively. The lowest detection limits for glucose as estimated based on three times of standard deviation from the blank were 9.3 μM and 23.4 μM for the GCE/TiO_2 NW/PAPBA–Au TNC (Fig. 8c(i)) and GCE/PAPBA–Au NC (Fig. 8c(ii)) electrodes, respectively. The new ISO 15197:2013 standard (as applicable from May 2016 onwards) suggests the accuracy of blood glucose test strips within ±20% of laboratory results for glucose concentrations > 5.6 mM and within ±0.83% for glucose concentrations < 5.6 mM. The ISO 15197:2013 fixes a limit of detection as 166 μM for glucose concentration levels below 5.6 mM. The lowest detection limit for glucose at the GCE/TiO_2 NW/PAPBA–Au TNC is 9.3 μM, which satisfies the 15197:2013 requirement for a strip glucose sensor. The sensitivity of GCE/TiO_2 NW/PAPBA–Au TNC (66.8 μA cm^{-2} mM^{-1}; Fig. 8c(i)) electrode was ~2 times higher than the sensitivity at PAPBA–Au NC (34.6 μA cm^{-2} mM^{-1}; Fig. 8c(ii)) electrode. The sensitivity, and linear range of the GCE/TiO_2 NW/PAPBA–Au TNC based glucose sensor are much superior to that of other reported glucose sensors based on TiO_2, Au NP, PANI and enzyme and its composites (Table 1).

Our results reveal that TiO_2 NW/PAPBA–Au TNC exhibits superior electroactivity, higher electrochemical surface area, faster electron transfer kinetics, and interfacial characteristics as compared to the pristine components. Also, it exhibits the highest glucose sensing performances as compared to the TiO_2 based materials reported in the literature (Table 1). We attribute

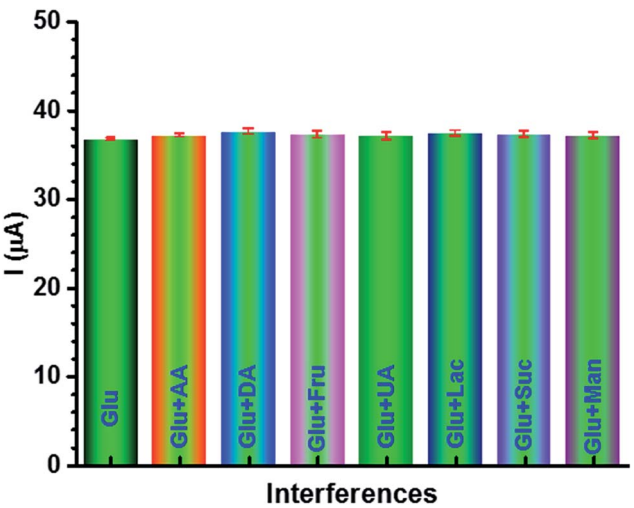

Fig. 9 DPV current responses at the GCE/TiO_2 NW/PAPBA–Au TNC electrode for 0.1 M PBS (pH 7.0) containing 1.0 mM glucose in the presence of 1.0 mM each ascorbic acid (AA), uric acid (UA) dopamine (DA), fructose (Fru), lactose (Lac), sucrose (Suc) and mannose (Mon). Scan rate: 50 mV s^{-1}, pulse amplitude: 50 mV, pulse width: 50 ms.

Table 2 Recovery of glucose in human serum samples at the GCE/TiO_2 NW/PAPBA–Au TNC electrode

Sample	Added glucose [mM]	Concentration [mM] Determined by glucometer	Determined at the fabricated electrode	Recovery [%]	RSD[a] [%]
Human serum samples	0	4.44 ± 0.01	4.43 ± 0.04	99.8	
	1	5.415 ± 0.06	5.412 ± 0.01	99.94	
	1	5.44 ± 0.02	5.43 ± 0.05	99.81	
	1	5.43 ± 0.07	5.413 ± 0.04	99.68	
	2	6.43 ± 0.03	6.425 ± 0.07	99.92	
	2	6.36 ± 0.01	6.358 ± 0.02	99.97	
	2	6.383 ± 0.05	6.38 ± 0.03	99.95	
	3	7.388 ± 0.3	7.37 ± 0.01	99.75	2.84
	3	7.34 ± 0.03	7.35 ± 0.07	100.13	
	3	7.442 ± 0.04	7.31 ± 0.06	98.22	
	4	8.41 ± 0.01	8.43 ± 0.02	100.23	
	4	8.45 ± 0.06	8.442 ± 0.05	99.90	
	4	8.378 ± 0.02	8.4 ± 0.04	100.26	
	5	9.42 ± 0.07	9.431 ± 0.03	100.11	
	5	9.39 ± 0.03	9.388 ± 0.04	99.97	
	5	9.41 ± 0.05	9.414 ± 0.03	100.04	

[a] Number of measurements = 3.

a multisource synergistic electrocatalytic effect for TiO_2 NW/PAPBA–Au TNC arising from the catalytic activity of TiO_2 NW in axial and radial directions and deliberate dispersion of electrocatalytic nanosized Au particles onto the electron mediating conducting polymer (PAPBA) having boronic acid binding groups to selectively bind glucose.

3.3.2. Selectivity. The selectivity of the sensor in an essential requirement for the practical application of electrochemical glucose sensor. We evaluated the selectivity of the proposed TiO_2 NW/PAPBA–Au TNC sensor towards 1 mM of glucose current response upon addition of 0.1 M of the commonly coexisting interfering species such as ascorbic acid (AA), uric acid (UA) dopamine (DA), fructose (Fru), lactose (Lac), sucrose (Suc) and mannose (Mon). The current responses were measured at 0.47 V. As shown in Fig. 9, it can be noticed that GCE/TiO_2 NW/PAPBA–Au TNC electrode exhibited nearly negligible current response with the addition of 0.1 mM of each interfering species. The results inform that the interfering substances contribute nearly 0.5–2.2% of the Δi value with respect to the current corresponding to 1 mM glucose. The result suggested that TiO_2 NW/PAPBA–Au TNC possessed excellent selectivity for the glucose detection.

3.3.3. Real sample analysis. In order to validate the GCE/TiO_2 NW/PAPBA–Au TNC electrode for the practical application of glucose monitoring in blood serum samples, the fabricated sensor was used for the detection of glucose in human blood serum samples. The glucose level in the human blood serum sample was pre-determined as 4.44 mM through a commercial glucometer (CareCens™ N, GM5051A, I-SENS, Inc., Korea) using a glucose strip. To evaluate the reproducibility of GCE/TiO_2 NW/PAPBA–Au TNC electrode, three different electrodes prepared under the same conditions were tested to detect the serum sample having a glucose concentration of 4.44 mM (against commercial glucometer). The average relative standard deviation (% RSD) was estimated to be lesser than 5%. Similarly, we tested sensor performance of the particularly fabricated sensor for the determination of glucose in serum for three times using the DPV calibration curve (Fig. 8c(i)). The previously tested sensor was gently rinsed with the buffer solution after each measurement. The results showed an average glucose concentration of 4.43 ± 0.04 mM with an RSD = 2.68%. Besides, the accuracy of the fabricated sensor was tested for the serum samples spiked with 1 mM, 2 mM, 3 mM, 4 mM and 5 mM of standard glucose independently to the serum samples (Table 2). Each serum sample was spiked for three times. A good recovery (98.2–100.26% with an RSD = 2.84%) towards glucose was obtained at GCE/TiO_2 NW/PAPBA–Au TNC electrode. We compared the determination results in blood samples detected from our experiments with those measured by the commercial glucometer and results are listed in Table 2. This comparison indicates that the results obtained by electrochemical detection at the GCE/TiO_2 NW/PAPBA–Au TNC electrode match well with those obtained by a routine commercially available glucose strip. Thus, we demonstrate the reproducibility and accuracy of GCE/TiO_2 NW/PAPBA–Au TNC electrode for the detection of glucose practical samples.

4. Conclusion

The ternary nanocomposite (TNC), comprising of the surface area enriched 1D TiO_2-NWs, a glucose binding conducting polymer (PAPBA) and electrocatalytic Au NPs materials was utilized for the construction of a sensitive non-enzymatic glucose sensor. The TiO_2 NW/PAPBA–Au TNC exhibited good sensor characteristics towards electrochemical detection of glucose. The TiO_2 NW/PAPBA–Au TNC sensor outperforms the

reported TiO_2 based glucose sensors. The peak current for glucose oxidation showed a linear dependence with a concentration of glucose in a wider range, 50 μM to 11 mM with a high sensitivity (66.8 μA cm^{-2} mM^{-1}). The excellent sensor performances (high sensitivity and wider linear range) at TiO_2 NW/PAPBA–Au TNC are due to synergistic roles of the components (TiO_2 NW, PAPBA, and Au NPs) in the newly synthesized TNC. Importantly, the peak current of glucose oxidation current was not influenced at TiO_2 NW/PAPBA–Au TNC in the presence of electrochemical interfering substances, such as ascorbic acid (AA), uric acid (UA) dopamine (DA), fructose (Fru), lactose (Lac), sucrose (Suc) and mannose (Mon). To note, TiO_2 NW/PAPBA–Au TNC sensor exhibited a remarkable performance in the human serum sample and signifies its utility for practical blood glucose detection.

Conflicts of interest

There are no conflicts to declare.

Acknowledgements

This work was supported by the Priority Research Center Program through a National Research Foundation of Korea (NRF) grant funded by the Ministry of Education, Science, and Technology (2009-0093819) and National Research Foundation of Korea (2014-R1A1A4A03004026).

References

1 A. Heller and B. Feldman, *Chem. Rev.*, 2008, **108**, 2482–2505.
2 C. Chen, Q. Xie, D. Yang, H. Xiao, Y. Fu, Y. Tan and S. Yao, *RSC Adv.*, 2013, **3**, 4473–4491.
3 A. S. Kumar, P. Y. Chen, S. H. Chien and J. M. Zen, *Electroanalysis*, 2005, **17**, 210–222.
4 D. P. Manica, Y. Mitsumori and A. G. Ewing, *Anal. Chem.*, 2003, **75**, 4572–4577.
5 S. Komathi, A. I. Gopalan, N. Muthuchamy and K. P. Lee, *RSC Adv.*, 2017, **7**, 15342–15351.
6 B. K. Jena and C. R. Raj, *Chem.–Eur. J.*, 2006, **12**, 2702–2708.
7 W. Liu, X. Wu and X. Li, *RSC Adv.*, 2017, **7**, 36744–36749.
8 X. Bo, J. C. Ndamanisha, J. Bai and L. Guo, *Talanta*, 2010, **82**, 85–91.
9 L. M. Lu, H. B. Li, F. Qu, X. B. Zhang, G. L. Shen and R. Q. Yu, *Biosens. Bioelectron.*, 2011, **26**, 3500–3504.
10 F. Cao, S. Guo, H. Ma, D. Shan, S. Yang and J. Gong, *Biosens. Bioelectron.*, 2011, **26**, 2756–2760.
11 C. Karuppiah, S. Palanisamy, S. M. Chen, V. Veeramani and P. Periakaruppan, *Sens. Actuators, B*, 2014, **196**, 450–456.
12 L. Xu, Q. Yang, X. Liu, J. Liu and X. Sun, *RSC Adv.*, 2014, **4**, 1449–1455.
13 N. Q. Dung, D. Patil, H. Jung and D. Kim, *Biosens. Bioelectron.*, 2013, **42**, 280–286.
14 A. I. Gopalan, N. Muthuchamy, S. Komathi and K. P. Lee, *Biosens. Bioelectron.*, 2016, **84**, 53–63.
15 A. I. Gopalan, N. Muthuchamy and K. P. Lee, *Biosens. Bioelectron.*, 2017, **89**, 352–360.
16 J. Yang, L. C. Jiang, W. D. Zhang and S. Gunasekaran, *Talanta*, 2010, **82**, 25–33.
17 G. Gnana Kumar, G. Amala and S. M. Gowtham, *RSC Adv.*, 2017, **7**, 36949–36976.
18 X. Lu, G. Wang, T. Zhai, M. Yu, J. Gan, Y. Tong and Y. Li, *Nano Lett.*, 2012, **12**, 1690–1696.
19 L. Hu, K. Huo, R. Chen, B. Gao, J. Fu and P. K. Chu, *Anal. Chem.*, 2011, **83**, 8138–8144.
20 P. V. Suneesh, V. S. Vargis, T. Ramachandran, B. G. Nair and T. S. Babu, *Sens. Actuators, B*, 2015, **215**, 337–344.
21 H. D. Jang, S. K. Kim, H. Chang, K. M. Roh, J. W. Choi and J. Huang, *Biosens. Bioelectron.*, 2012, **38**, 184–188.
22 Z. D. Gao, Y. Han, Y. Wang, J. Xu and Y. Y. Song, *Sci. Rep.*, 2013, **3**, 3323.
23 L. Tian, W. Hu, X. Zhong and B. Liu, *Mater. Res. Innovations*, 2015, **3**, 160–165.
24 X. Chen, G. Li, G. Zhang, K. Hou, H. Pan and M. Du, *Mater. Sci. Eng., C*, 2016, **62**, 323–328.
25 X. Y. Lang, H. Y. Fu, C. Hou, G. F. Han, P. Yang, Y. B. Liu and Q. Jiang, *Nat. Commun.*, 2013, **4**, 2169.
26 X. C. Dong, H. Xu, X. W. Wang, Y. X. Huang, M. B. Chan-Park, H. Zhang, L. H. Wang, W. Huang and P. Chen, *ACS Nano*, 2012, **6**, 3206–3213.
27 J. Z. Chen, W. Y. Ko, Y. C. Yen, P. H. Chen and K. J. Lin, *ACS Nano*, 2012, **6**, 6633–6639.
28 S. Komathi, N. Muthuchamy, K. P. Lee and A. I. Gopalan, *Biosens. Bioelectron.*, 2016, **84**, 64–71.
29 N. Muthuchamy, K. P. Lee and A. I. Gopalan, *Biosens. Bioelectron.*, 2017, **89**, 390–399.
30 B. Deore and M. S. Freund, *Analyst*, 2003, **128**, 803–806.
31 X. Wang, Y. Liu, L. Ren, H. Li and Z. Liu, *Anal. Methods*, 2013, **5**, 5444–5449.
32 S. Badhulika, C. Tlili and A. Mulchandani, *Analyst*, 2014, **139**, 3077–3082.
33 H. Torul, H. Çiftçi, F. C. Dudak, Y. Adıgüzel, H. Kulah, İ. H. Boyacı and U. Tamer, *Anal. Methods*, 2014, **6**, 5097–5104.
34 Q. Wu, L. Wang, H. Yu, J. Wang and Z. Chen, *Chem. Rev.*, 2011, **111**, 7855–7875.
35 D. G. Hall, *Boronic Acids: Preparation and Applications in Organic Synthesis, Medicine, and Materials*, Wiley-VCH, Weinheim, Germany, 2011.
36 R. Nishiyabu, Y. Kubo, T. D. James and J. S. Fossey, *Chem. Commun.*, 2011, **47**, 1106.
37 K. M. Manesh, P. Santhosh, A. Gopalan and K. P. Lee, *Anal. Biochem.*, 2007, **360**, 189–195.
38 K. L. Adams, B. K. Jena, S. J. Percival and B. Zhang, *Anal. Chem.*, 2011, **83**, 920–927.
39 X. Zhang, T. Zeng, C. Hu and S. Hu, *Anal. Methods*, 2016, **8**, 1162–1169.
40 P. Daggumati, Z. Matharu and E. Seker, *Anal. Chem.*, 2015, **87**, 8149–8156.
41 S. D. Bull, M. G. Davidson, J. M. Van den Elsen, J. S. Fossey, A. T. A. Jenkins, Y. B. Jiang, Y. Kubo, F. Marken, K. Sakurai, J. Zhao and T. D. James, *Acc. Chem. Res.*, 2012, **46**, 312–326.
42 A. Pandya, P. G. Sutariya and S. K. Menon, *Analyst*, 2013, **138**, 2483–2490.

43 H. G. Lee, G. Sai-Anand, S. Komathi, A. I. Gopalan, S. W. Kang and K. P. Lee, *J. Hazard. Mater.*, 2015, **283**, 400–409.
44 M. Zhao, X. Wu and C. Cai, *J. Phys. Chem. C*, 2009, **113**, 4987–4996.
45 C. Xiang, Y. Zou, S. Qiu, L. Sun, F. Xu and H. Zhou, *Talanta*, 2013, **110**, 96–100.
46 Z. Wang, S. Liu, P. Wu and C. Cai, *Anal. Chem.*, 2009, **81**, 1638–1645.
47 W. Tang, L. Li and X. Zeng, *Talanta*, 2015, **131**, 417–423.
48 X. Y. Pang, D. M. He, S. L. Luo and Q. Y. Cai, *Sens. Actuators, B*, 2009, **137**, 134–138.
49 J. H. Lopes, F. X. Colson, J. E. Barralet and G. Merle, *Mater. Sci. Eng. C*, 2017, **76**, 991–996.
50 N. Q. Dung, D. Patil, T. T. Duong, H. Jung, D. Kim and S.-G. Yoon, *Sens. Actuators, B*, 2012, **166–167**, 103–109.
51 M. Long, L. Tan, H. Liu, Z. He and A. Tang, *Biosens. Bioelectron.*, 2014, **59**, 243–250.
52 C. Feng, G. Xu, H. Liu, J. Lv, Z. Zheng and Y. Wu, *J. Solid State Electrochem.*, 2014, **18**, 163–171.
53 C. Feng, G. Xu, H. Liu, J. Lv, Z. Zheng and Y. Wu, *J. Electrochem. Soc.*, 2014, **161**, B1–B8.
54 Z. Zhang, Y. Xie, Z. Liu, F. Rong, Y. Wang and D. Fu, *J. Electroanal. Chem.*, 2011, **650**, 241–247.
55 C. Jiang, J. Zhu, Z. Li, J. Luo, J. Wang and Y. Sun, *RSC Adv.*, 2017, **7**, 44463–44469.
56 P. Si, S. J. Ding, J. Yuan, X. W. Lou and D. H. Kim, *ACS Nano*, 2011, **5**, 7617–7626.
57 Q. Guo, L. Liu, M. Zhang, H. Hou, Y. Song, H. Wang, B. Zhong and L. Wang, *Biosens. Bioelectron.*, 2017, **92**, 654–660.
58 A. I. Gopalan, K.-P. Lee, D. Ragupathy, S.-H. Lee and J.-W. Lee, *Biomaterials*, 2009, **30**, 5999–6005.